RESEARCH ARTICLE | FEBRUARY 19 2025

Acoustic non-Hermitian higher-order topological bound states in the continuum

Haiyan Fan ; He Gao ; Tuo Liu ; Shuowei An ; Yifan Zhu ; Hui Zhang ; Jie Zhu ; Zhongqing Su

Appl. Phys. Lett. 126, 071702 (2025)
https://doi.org/10.1063/5.0249792

Applied Physics Letters ARTICLE pubs.aip.org/aip/apl

Acoustic non-Hermitian higher-order topological bound states in the continuum

Cite as: Appl. Phys. Lett. **126**, 071702 (2025); doi: 10.1063/5.0249792
Submitted: 20 November 2024 · Accepted: 27 January 2025 ·
Published Online: 19 February 2025

Haiyan Fan,[1] He Gao,[2,a)] Tuo Liu,[3,a)] Shuowei An,[2] Yifan Zhu,[1] Hui Zhang,[1] Jie Zhu,[4,5] and Zhongqing Su[2,a)]

AFFILIATIONS

[1]Jiangsu Key Laboratory for Design and Manufacture of Micro-Nano Biomedical Instruments, School of Mechanical Engineering, Southeast University, Nanjing 211189, China
[2]Department of Mechanical Engineering, The Hong Kong Polytechnic University, Hung Hom, Kowloon, Hong Kong SAR, People's Republic of China
[3]Institute of Acoustics, Chinese Academy of Sciences, Beijing 100190, China
[4]Institute of Acoustics, School of Physics Science and Engineering, Tongji University, Shanghai 200092, China
[5]Shanghai Research Institute for Intelligent Autonomous Systems, Tongji University, Shanghai 201210, China

[a)]**Authors to whom correspondence should be addressed:** h.e.gao@connect.polyu.hk; liutuo@mail.ioa.ac.cn; and zhongqing.su@polyu.edu.hk

ABSTRACT

Recently, the concept of bound states in the continuum (BICs) has been extended to topological physics, inspiring investigations into higher-order topological BICs (TBICs) and related ultra-strong wave localization, which not only enriches the realm of topological physics but also bestows the BICs with inherent topological protection. However, previous explorations toward higher-order TBICs have been limited to the Hermitian assumption, omitting the nonconservative characteristics present in many artificial materials. In this work, we propose and experimentally demonstrate an acoustic lattice model supporting higher-order TBICs that solely rely on non-Hermiticity, in which the non-Hermiticity is implemented by strategically applying additional loss to specific sites in the lattice. Importantly, these in-band corner states are protected by chiral symmetry and can be spectrally switched by introducing perturbations to the corner sites or couplings. Our findings highlight the distinctive role of non-Hermiticity in constructing higher-order TBICs, which may inspire sophisticated and externally tunable approaches for designing high-Q devices in wave-based technologies.

Topological physics has revolutionized the understanding and exploitation of both natural materials[1–3] and artificial structures[4–8] in the past two decades. Among various artificial structures, those based on acoustic systems offer a unique platform for exploring richer topological phenomena that are difficult to observe in natural materials. One prominent example is higher-order topological insulators (HOTIs) that exhibit a hierarchy of multidimensional nontrivial topological states governed by the bulk multipole moments,[9,10] nontrivial dipole polarizations,[11–13] or multidimensional topological phase transitions.[14,15] These studies typically rely on Hermitian descriptions, assuming energy conservation. However, acoustic systems inevitably experience intrinsic losses due to thermoviscous and viscoelastic effects, rendering the Hermitian Hamiltonian inaccurate in realistic scenarios.

While conventional wisdom suggests that energy decay due to losses hinders the observation of topological states, recent research has focused on the intriguing interplay between non-Hermiticity and band topology.[16–18] This has led to the discovery of gapless topological phases with exceptional degeneracies[19,20] and gapped non-Hermitian topology.[21,22] Non-Hermitian HOTIs have been theoretically predicted[23,24] and experimentally validated,[25] showcasing nontrivial bandgaps in which higher-order topological corner states emerge.

Although most of the higher-order topological states reside in the nontrivial bandgaps to isolate the spatially localized states from the continuous spectra, bandgaps are not indispensable for constructing higher-order topological states.[26] When they exist within the bulk band, the so-called higher-order topological BIC (TBIC) is formed.[27,28] Bound states in the continuum (BICs) are spatially localized eigenstates coexisting with continuous spectra of propagating eigenstates.[29] The combination of BICs and topological phases gives rise to TBICs that inherit both topological protection and localization, even in the

presence of continuous spectra. This has spurred extensive research on TBICs, ranging from in-band first-order topological edge states[30,31] to higher-order TBICs.[32–35] The physical mechanisms underlying TBICs can be categorized into three main approaches: eigenfrequency shift due to coupling adjustment,[30,31] mirror-stacking,[33] and onsite non-Hermitian modulations.[36,37] Specific to acoustic systems, TBICs under non-Hermitian modulations stand out as more realistic scenarios as compared to the first two approaches in view of the ubiquitous thermoviscous loss effect, but previous studies have been limited to the one-dimensional (1D) regime.

In this work, we present a theoretical and experimental investigation of higher-order TBICs in two-dimensional (2D) acoustic lattices with uneven onsite loss modulations. As the onsite loss increases, the original extended bulk states gradually evolve into localized edge and corner states. Notably, the corner states remain pinned at the zero-energy within the middle bulk band region, exhibiting the characteristics of higher-order TBICs. The nonzero 2D polarizations calculated from the bulk bands suggest the topological protection of theses TBICs. Perturbations on the cavities or linked tubes can shift the eigenfrequencies of the TBICs and even pull them out of the bands. Such an approach of constructing and tuning non-Hermiticity-induced higher-order TBICs can not only enhance the practical applicability of TBICs in acoustics but also simplify their implementation by allowing flexible adjustment of onsite non-Hermiticities through external methods, eliminating the need for structural modifications.

To elucidate our basic ideas, we consider a 2D lattice with a tight-binding Hamiltonian written as

$$H = \sum_{n=1}^{N}\sum_{m=1}^{M}(-i\gamma_{n,m})\, c_{n,m}^{\dagger}c_{n,m} + \sum_{n=1}^{N-1}\sum_{m=1}^{M-1}(t_x c_{n,m}^{\dagger}c_{n+1,m} + t_y c_{n,m}^{\dagger}c_{n,m+1} + \text{H.c.}), \quad (1)$$

where $c_{n,m}^{\dagger}(c_{n,m})$ represents the creation (annihilation) operator on the (n, m) site, $t_x(t_y)$ is the hopping term along the $x(y)$-direction, and H.c. stands for Hermitian conjugate. In the basic unit cell [3×3 atoms, as encircled by the dotted square in Fig. 1(a)], the on-site losses, $\gamma_{n,m}$, take the value of γ_2 for $(m,n) = (2i - 1, 2j - 1)$ $(i,j = 1,2)$ and γ_1 for the remaining sites. To identify the in-band corner and edge eigenenergy, a corner localization coefficient α and an edge localization coefficient β are defined as

$$\alpha = \left(\xi_{1,1}^2 + \xi_{1,M}^2 + \xi_{N,1}^2 + \xi_{N,M}^2\right) \Big/ \sum_{n=1}^{N}\sum_{m=1}^{M}\xi_{n,m}^2$$

$$\beta = \Bigg[\sum_{n=1}^{N}(\xi_{n,1}^2 + \xi_{n,M}^2) + \sum_{m=1}^{M}(\xi_{1,m}^2 + \xi_{N,m}^2) - 2(\xi_{1,1}^2 + \xi_{1,M}^2 + \xi_{N,1}^2 + \xi_{N,M}^2) - \sum_{i=0}^{N/3-1}(\xi_{2+3i,1}^2 + \xi_{2+3i,M}^2) - \sum_{j=0}^{M/3-1}(\xi_{1,2+3j}^2 + \xi_{M,2+3j}^2)\Bigg] \Big/ \sum_{n=1}^{N}\sum_{m=1}^{M}\xi_{n,m}^2. \quad (2)$$

In the equations, $\xi_{n,m}$ represents the wavefunction on the (n, m) site. Figure 1(b) shows the evolution of the calculated real parts of eigenenergy with the increase in loss contrast ($\Delta\gamma = \gamma_2 - \gamma_1$) in a finite lattice, and the corresponding corner and edge localization coefficients are denoted by the red and blue color bar, respectively. The ratio between loss contrast ($\Delta\gamma$) and hopping term (t) is critical for the emergence of higher-order non-Hermitian TBICs. When $\Delta\gamma = 0$, no bandgaps or concentrated edge and corner localizations can be observed in the eigenenergy spectrum of the finite-sized lattice, as presented in Fig. 1(b). With increasing $\Delta\gamma$, bandgaps gradually appear and stabilize once the ratio reaches a characteristic value of $\Delta\gamma/t = 3.4$. Simultaneously, the corner states become pinned at the zero-energy, signifying the formation of higher-order TBICs. These higher-order TBICs exhibit fractional corner charges and filling anomalies, consistent with the behavior observed in higher-order topological insulators with bandgaps.[38] Following the scheme of calculating electron density at "half-filling,"[10] quantized fractional charges are observed at the four corners in this non-Hermitian finite model by accumulating the lower half of eigenstates in space [Fig. 1(c)].

The above tight-binding model (TBM) can be realized using periodically arranged acoustic coupled cavities, each unit cell of which consists of nine resonant cavities connected by thin tubes, as sketched in Fig. 2(a). The cavities in blue have a higher loss coefficient (γ_2), while

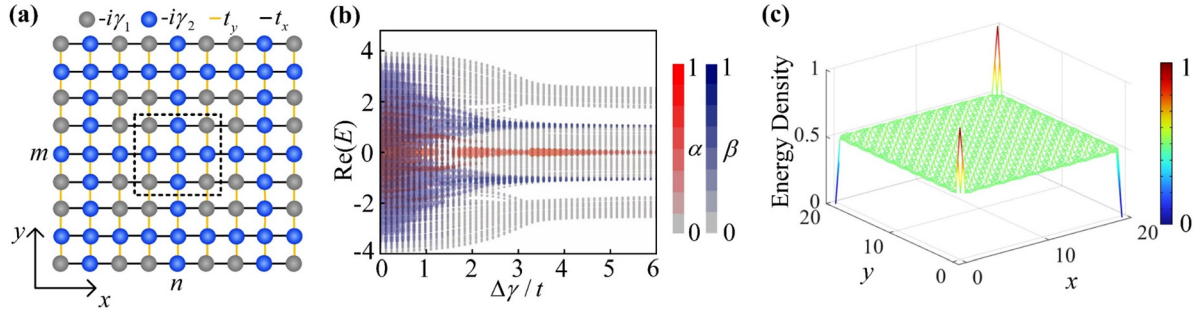

FIG. 1. In-band topological corner states for a finite-sized TBM with non-Hermitian modulation. (a) The finite-sized TBM. Sites colored in gray (blue) have lower loss γ_1 (higher loss γ_2). The hopping terms in the x and y directions are represented by the black lines (t_x) and orange lines (t_y), respectively. The dotted black square encircles a minimal unit cell. (b) The real parts of the complex eigenenergy as a function of loss contrast, $\Delta\gamma = \gamma_2 - \gamma_1$, for the model illustrated in (a). The red (blue) color bar represents the value of corner localization coefficient α (edge localization coefficient β). In the calculations $N = 24$, $M = 24$, $\gamma_1 = 0$, and $t_x = t_y = t = 1$. (c) The sum of the lower half eigenstates, indicating fractional corner charges (0.5 ± 0.5) at four corner sites.

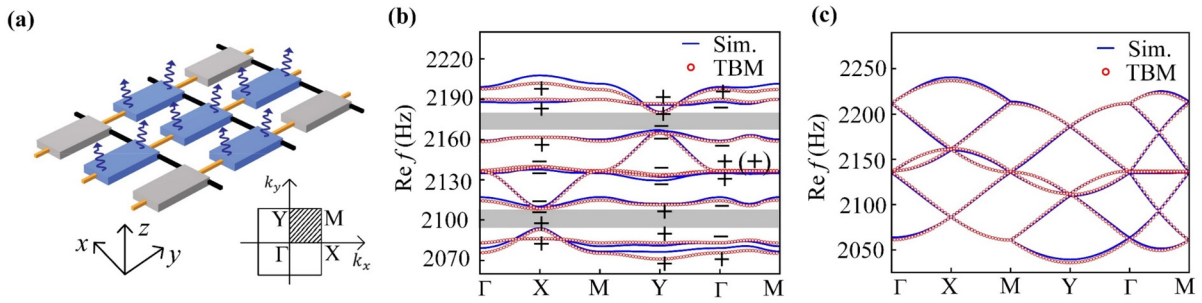

FIG. 2. Acoustic unit cell and band structures. (a) A schematic of a unit cell with nine cavities and linked tubes. Every cavity (tube) has the same dimensions of $80 \times 40 \times 10\,\text{mm}^3$ ($40 \times 4 \times 4\,\text{mm}^3$). (b) Band structure of the unit cell in (a) with marked parities at X, Y, and Γ. Symbol + (−) denotes even (odd) parity, which can be determined by their eigenstates. (c) Band structure of the unit cell without additional loss. The blue lines are the simulated results, and the red circles show the calculated results based on TBM.

those in gray have a lower loss coefficient (γ_1). The cavity array forms a rectangular lattice that satisfies C_{2v} symmetry, and the corresponding first Brillouin zone (BZ) is given in the inset of Fig. 2(a). The effective loss coefficients are $\gamma_1 = 13.3\,\text{Hz}$ and $\gamma_2 = 128.5\,\text{Hz}$,[39] and the hopping terms along the x and y directions are $t_x = -25.0\,\text{Hz}$ and $t_y = 25.3\,\text{Hz}$ (a trivial difference in hopping strength between the two terms is due to the mode shape of the cavity, see Ref. 25), giving rise to $\Delta\gamma/t \approx 4.6$. Figure 1(b) demonstrates a clear separation between the in-band corner states and edge states at this value, providing a suitable foundation for further observations. Under these parameters, the simulated band structure of the unit cell with (without) additional loss is denoted by the blue lines in Fig. 2(b) [Fig. 2(c)], consistent with the results based on tight-binding calculations represented by the red circles in Fig. 2(b) [Fig. 2(c)]. The introduction of additional loss leads to the opening of two bandgaps [Fig. 2(b)] within the originally closed band structure [Fig. 2(c)].

The topological properties can be characterized by the extended Zak phase in 2D, which can also be represented by the 2D polarization $P = (P_x, P_y)$ given by Refs. 32 and 40,

$$P_i = \frac{1}{2}\left(\sum_n q_i^n \bmod 2\right), \ (-1)^{q_i^n} = \frac{\eta_n(A_i)}{\eta_n(\Gamma)}, \tag{3}$$

where $i = x, y$, η_n is the parity at the high symmetry points (X, Y, and Γ) in BZ for the nth band, $\sum_n q_i^n$ denotes the summation over the occupied bands, and mod means the modulo operation. According to the marked parity at Γ and X (Y) in Fig. 2(b), both the first and second bandgaps, marked by the gray shadows, possess quantized dipole moment of $P_x = 1/2$ ($P_y = 1/2$), as there are odd numbers of parity-inverted bands between the Γ and X (Y) points below the bandgaps. As presented in Fig. 2(c), these bandgaps will disappear in the absence of loss contrast, highlighting the crucial role of non-Hermiticity in their formation. While non-Hermiticity can induce topological bandgaps, the emergence of associated topological states within these gaps is not guaranteed.

We calculate the complex spectrum for the finite-sized acoustic lattice composed of 12×12 cavities based on the above-mentioned unit cell, as shown in Fig. 3(a). From the distribution of the bulk states (gray dots), an obvious imaginary frequency gap, ranging from 33 to 93 Hz, can be observed due to the uneven losses between the two types of cavities. Two real frequency gaps are opened among the three bulk regions, where the edge states (blue dots) appear with lower imaginary parts. The corner states (red dots) are found embedded in the middle bulk region with lower imaginary parts.

To numerically investigate the spatial responses of the non-Hermitian system, a monopole source is applied at the positions marked by the red, blue, and gray arrows in Fig. 3(b), in order to excite the higher-order TBICs, edge states, and bulk states, respectively. When the source with an operating frequency of 2138 Hz is located at the corner cavity, the sound field is strongly confined to the corner [left panel in Fig. 3(b)] as a result of the excitation of the corner state. As the source is moved to the inner bulk of the system, the sound field generated by the source decays spatially but more moderately as compared to the case of the corner source due to both geometric and physical (non-Hermiticity) attenuations in the bulk [left panel in Fig. 3(b)]. These results indicate that the topological corner states coexist with the bulk states, forming the so-called higher-order TBICs. In addition, when the excitation signal with a frequency of 2164 Hz is placed at one of the system's boundaries, the sound field is localized at the boundary and attenuates (also owing to non-Hermiticity) along the boundary, as shown in the middle panel in Fig. 3(b), indicating that the topological edge states are created with the addition of extra loss.

To experimentally validate the existence of non-Hermitian higher-order TBICs, we measure the acoustic responses of the experimental sample with uneven losses. As presented in Fig. 4(a), sound absorptive materials are inserted into small holes in the cavities to introduce additional loss. First, a loudspeaker and a microphone are placed at a bulk cavity [labeled as "3" in Fig. 4(a)] to examine the bandgap property. The measured response spectrum, as given by the gray shading in Fig. 4(b), exhibits three distinct peaks separated by two gaps, consistent with the three regions of bulk states with lower imaginary parts in Fig. 3(a). Next, we excite an edge cavity [marked as "2" in Fig. 4(a)] and measure its response spectrum. As indicated by the blue shading in Fig. 4(b), two peaks appear within the intervals of the gray shading, confirming the numerical prediction of edge states in Fig. 3(a). The corner response spectrum, measured in cavity "1" in Fig. 4(a) and denoted by the red shading in Fig. 4(b), exhibits only one peak. Notably, this peak shares the same frequency as the middle peak of the bulk spectrum, providing evidence that the topological corner states are embedded within the bulk bands.

To further confirm these findings, we repeat the measurements (both loudspeaker and microphone are placed at the same cavity) for

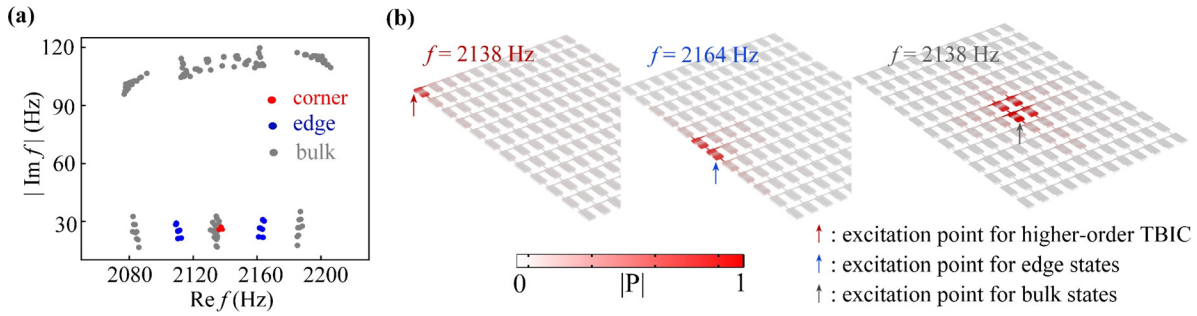

FIG. 3. Acoustic implementation of the non-Hermiticity-induced higher-order TBICs. (a) Simulated complex eigenfrequencies of an acoustic lattice with 12 × 12 cavities. The in-band topological corner states are denoted by red dots. Bulk and edge states are marked by gray and blue dots, respectively. (b) Acoustic spatial responses of the non-Hermitian lattice at frequencies of 2138 and 2164 Hz, with excitation source placed at the corner (red arrow), edge (blue arrow), and bulk (gray arrow), respectively.

all cavities and plot the site-resolved energy profiles at three peak frequencies [denoted by the dashed lines in Fig. 4(b)]. As expected, for different peak frequencies, the sound intensity field distributes within the bulk [Fig. 4(c)] or is localized at the edge [Fig. 4(d)] or corner [Fig. 4(e)] site, respectively. Note that such higher-order TBICs induced by onsite uneven losses can also be effectively described by the uneven coupling terms in the Hermitian case (see the supplementary material, note 1). All these experimental results show consistency with the simulated ones (see the supplementary material, note 2).

Interestingly, the higher-order TBICs can be spectrally shifted and even pulled out of the bulk bands by breaking the chiral symmetry through slight modifications of the resonance frequencies of the corner cavities. As illustrated in Fig. 5(a), we introduce varying volumes of water [blue area in the inset of Fig. 5(a)] into the corner cavities through a tiny hole, effectively decreasing their lengths.[41] This results in a gradual increase in the measured resonance frequencies of the corner sites $f_0 = c/2(D-h)$, where c is the speed of sound speed in air, $D = 80$ mm is the length of the corner cavity, and h is the depth of water. Correspondingly, the measured frequencies of the corner states in the acoustic lattices, denoted by the red circles in Fig. 5(b), increase synchronously with the increased water depth, even when located within a bandgap. These experimental results are consistent with the numerically calculated eigenfrequencies of topological corner states, marked by the red solid line in Fig. 5(b).

Furthermore, the eigenfrequencies of the corner states can also be tuned by adjusting the length of the connecting tubes in the acoustic lattice. As given in Fig. 5(c), the resonance frequencies of the corner cavities decrease gradually with increasing tube length. Notably, the corner states appear at the zero-energy frequency ($f_0 = 2138$ Hz) only when $l = 40$ mm, where the chiral symmetry is protected for the 2D linked acoustic cavity system. In contrast to adding perturbations to the onsite cavities, which only affects the frequencies of corner states [Fig. 5(b)], the spectral position of all states can be controlled by changing l [Fig. 5(d)]. For instance, when $l = 22$ mm, the corner states

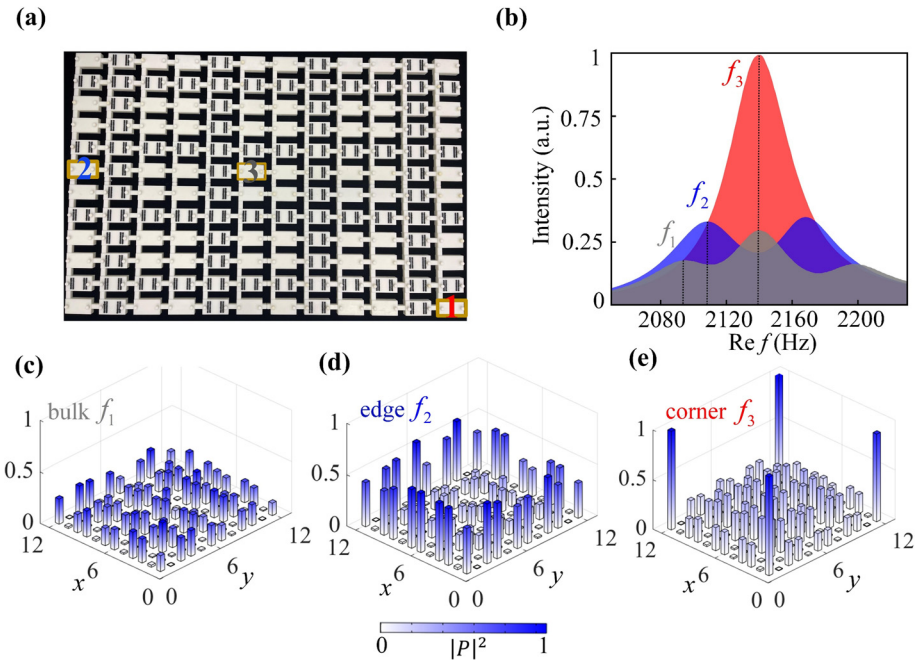

FIG. 4. Experimental responses of the non-Hermitian lattice with uneven losses. (a) A bird's-eye view of the experimental sample with 12 × 12 cavities. Additional loss is introduced by inserting sound absorptive material (black sponge) into the cavities. (b) Measured frequency spectra at corner cavity 1 (red), edge cavity 2 (blue), and bulk cavity 3 (gray), as labeled in (a). (c)–(e) Measured spatial distributions of sound intensity fields at the peak frequencies of the bulk ($f_1 = 2093$ Hz), edge ($f_2 = 2109$ Hz), and corner ($f_3 = 2138$ Hz) spectra, respectively. Both the color and height of the bar denote the intensity.

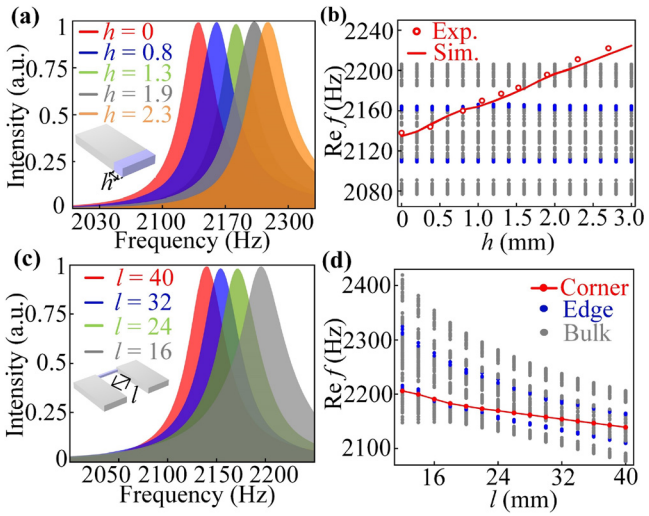

FIG. 5. Tunability of the higher-order TBICs. (a) Measured response spectra at a corner cavity with different depths of water (h). The inset shows the cavity with pumped water. (b) The frequency evolution of corner states as a function of increasing water depth. The red circles depict the measured results, and the red curve represents the simulated results. The blue (gray) dots are simulated edge (bulk) states. (c) Simulated response spectra at a corner cavity with different lengths of tubes (l). The inset shows two cavities coupled with the linked tube. (d) Eigenfrequency evolution of the acoustic lattice as a function of the increasing tube length. The red line represents the simulated corner states. The blue (gray) dots are simulated edge (bulk) states.

are modulated to lie within a bandgap, and the eigenfrequencies of all states increase compared to the case when $l = 40$ mm.

We have proposed to apply acoustic loss to induce the higher-order TBICs, which have been numerically and experimentally demonstrated in a 2D coupled acoustic cavity system. Starting with an ideal TBM, the nontrivial topological phase in our system arises from the ratio between loss contrast and coupling strengths. In these C_{2v} symmetric lattices, the corner cavities are primarily excited within the middle bulk bands, implying that the corner states reside in these bands. Importantly, the frequencies of these in-band corner states can be flexibly tuned via perturbing the resonance frequencies of the corner cavities or the lengths of the connecting tubes. Our findings lift the requirement of the bandgap in probing topological physics and offer insights into the role that non-Hermiticity plays in constructing higher-order TBICs, which may inspire richer interactions between topology and BICs. Since the related tight-binding Hamiltonian has been experimentally realized in various platforms, this non-Hermitian scheme is generally extendable to electronic system,[42] microwave,[43] elastic lattices,[21] and optical waveguides[44] to explore more sophisticated topological phenomena.

See the supplementary material for the following: (1) uneven-coupling-induced higher-order topological bound states in the continuum; (2) simulated field intensity distribution of the non-Hermitian lattice; and (3) details for simulation and experiment.

This work was supported by grants from the Hong Kong Research Grants Council (Grant Nos. AoE/P-502/20 and 15200922) and the National Natural Science Foundation of China (Grant Nos. 92263208 and 12104383). Haiyan Fan acknowledges support from the Start-up Research Fund of Southeast University (Grant No. RF10286240107).

AUTHOR DECLARATIONS

Conflict of Interest

The authors have no conflicts to disclose.

Author Contributions

Haiyan Fan: Conceptualization (equal); Formal analysis (equal); Investigation (equal); Software (equal); Writing – original draft (equal); Writing – review & editing (equal). **He Gao:** Conceptualization (equal); Validation (equal); Writing – review & editing (equal). **Tuo Liu:** Conceptualization (equal); Supervision (equal); Writing – review & editing (lead). **Shuowei An:** Investigation (equal); Methodology (equal). **Yifan Zhu:** Methodology (equal); Writing – review & editing (equal). **Hui Zhang:** Methodology (equal); Writing – review & editing (equal). **Jie Zhu:** Project administration (lead); Writing – review & editing (equal). **Zhongqing Su:** Supervision (lead); Writing – review & editing (equal).

DATA AVAILABILITY

The data that support the findings of this study are available from the corresponding authors upon reasonable request.

REFERENCES

[1]F. D. M. Haldane, Rev. Mod. Phys. **89**, 040502 (2017).
[2]X.-L. Qi and S.-C. Zhang, Rev. Mod. Phys. **83**, 1057 (2011).
[3]M. Z. Hasan and C. L. Kane, Rev. Mod. Phys. **82**, 3045 (2010).
[4]Y. F. Chen, Z. G. Chen, H. Ge, C. He, X. Li, M. H. Lu, X. C. Sun, S. Y. Yu, and X. Zhang, Interdiscip. Mater. **2**, 179 (2023).
[5]H. Xue, Y. Yang, and B. Zhang, Nat. Rev. Mater. **7**, 974 (2022).
[6]M. Ling, Z. Xu, S. Wang, Y. Huang, and L. Wang, Appl. Phys. Lett. **124**, 161701 (2024).
[7]T. Ozawa, H. M. Price, A. Amo, N. Goldman, M. Hafezi, L. Lu, M. C. Rechtsman, D. Schuster, J. Simon, O. Zilberberg, and I. Carusotto, Rev. Mod. Phys. **91**, 015006 (2019).
[8]S. D. Huber, Nat. Phys. **12**, 621 (2016).
[9]W. A. Benalcazar, B. A. Bernevig, and T. L. Hughes, Phys. Rev. B **96**, 245115 (2017).
[10]W. A. Benalcazar, B. A. Bernevig, and T. L. Hughes, Science **357**, 61 (2017).
[11]X. Ni, M. Weiner, A. Alu, and A. B. Khanikaev, Nat. Mater. **18**, 113 (2019).
[12]H. Xue, Y. Yang, F. Gao, Y. Chong, and B. Zhang, Nat. Mater. **18**, 108 (2019).
[13]H. Fan, B. Xia, L. Tong, S. Zheng, and D. Yu, Phys. Rev. Lett. **122**, 204301 (2019).
[14]X. Zhang, H.-X. Wang, Z.-K. Lin, Y. Tian, B. Xie, M.-H. Lu, Y.-F. Chen, and J.-H. Jiang, Nat. Phys. **15**, 582 (2019).
[15]Y. Wu, M. Yan, Z. K. Lin, H. X. Wang, F. Li, and J. H. Jiang, Sci. Bull. **66**, 1959 (2021).
[16]Y. Ashida, Z. Gong, and M. Ueda, Adv. Phys. **69**, 249 (2021).
[17]M. Peng, C. Wu, Z. Cui, X. Zhang, Q. Wei, M. Yan, and G. Chen, Appl. Phys. Lett. **125**, 193101 (2024).
[18]X. Zhang, F. Zangeneh-Nejad, Z. G. Chen, M. H. Lu, and J. Christensen, Nature **618**, 687 (2023).
[19]Z. Zhu, S.-K. Jian, and D. N. Sheng, Phys. Rev. B **99**, 201108(R) (2019).
[20]K. Kawabata, K. Shiozaki, M. Ueda, and M. Sato, Phys. Rev. X **9**, 041015 (2019).
[21]H. Fan, H. Gao, S. An, Z. Gu, S. Liang, Y. Zheng, and T. Liu, Mech. Syst. Signal Process. **169**, 108774 (2022).

[22]B. Hu, Z. Zhang, H. Zhang, L. Zheng, W. Xiong, Z. Yue, X. Wang, J. Xu, Y. Cheng, X. Liu, and J. Christensen, Nature **597**, 655 (2021).
[23]T. Liu, Y. R. Zhang, Q. Ai, Z. Gong, K. Kawabata, M. Ueda, and F. Nori, Phys. Rev. Lett. **122**, 076801 (2019).
[24]X. W. Luo and C. Zhang, Phys. Rev. Lett. **123**, 073601 (2019).
[25]H. Gao, H. Xue, Z. Gu, T. Liu, J. Zhu, and B. Zhang, Nat. Commun. **12**, 1888 (2021).
[26]M. Zelenayova and E. J. Bergholtz, Appl. Phys. Lett. **124**, 041105 (2024).
[27]Y. Wang, B. Y. Xie, Y. H. Lu, Y. J. Chang, H. F. Wang, J. Gao, Z. Q. Jiao, Z. Feng, X. Y. Xu, F. Mei, S. Jia, M. H. Lu, and X. M. Jin, Light Sci. Appl. **10**, 173 (2021).
[28]A. Cerjan, M. Jurgensen, W. A. Benalcazar, S. Mukherjee, and M. C. Rechtsman, Phys. Rev. Lett. **125**, 213901 (2020).
[29]C. W. Hsu, B. Zhen, A. D. Stone, J. D. Joannopoulos, and M. Soljačić, Nat. Rev. Mater. **1**, 16048 (2016).
[30]S. Yin, L. Ye, H. He, X. Huang, M. Ke, W. Deng, J. Lu, and Z. Liu, Sci. Bull. **69**, 1660 (2024).
[31]Y. X. Xiao, G. Ma, Z. Q. Zhang, and C. T. Chan, Phys. Rev. Lett. **118**, 166803 (2017).
[32]F. Liu and K. Wakabayashi, Phys. Rev. Lett. **118**, 076803 (2017).
[33]L. Liu, T. Li, Q. Zhang, M. Xiao, and C. Qiu, Phys. Rev. Lett. **130**, 106301 (2023).
[34]W. A. Benalcazar and A. Cerjan, Phys. Rev. B **101**, 161116 (2020).
[35]T. L. C. W. Peterson, W. A. Benalcazar, T. L. Hughes, and G. Bahl, Science **368**, 1114 (2020).
[36]L. Jin, Phys. Rev. A **96**, 032103 (2017).
[37]H. Fan, H. Gao, S. An, Z. Gu, Y. Chen, S. Huang, S. Liang, J. Zhu, T. Liu, and Z. Su, Phys. Rev. B **106**, L180302 (2022).
[38]W. A. Benalcazar, T. Li, and T. L. Hughes, Phys. Rev. B **99**, 245151 (2019).
[39]H. Fan, H. Gao, T. Liu, S. An, X. Kong, G. Xu, J. Zhu, C.-W. Qiu, and Z. Su, Phys. Rev. B **107**, L201108 (2023).
[40]C. Fang, M. J. Gilbert, and B. A. Bernevig, Phys. Rev. B **86**, 115112 (2012).
[41]Z. Tian, C. Shen, J. Li, E. Reit, H. Bachman, J. E. S. Socolar, S. A. Cummer, and T. J. Huang, Nat. Commun. **11**, 762 (2020).
[42]S. Liu, S. Ma, C. Yang, L. Zhang, W. Gao, Y. J. Xiang, T. J. Cui, and S. Zhang, Phys. Rev. Appl. **13**, 014047 (2020).
[43]C. W. Peterson, W. A. Benalcazar, T. L. Hughes, and G. Bahl, Nature **555**, 346 (2018).
[44]H. Zhao, X. Qiao, T. Wu, B. Midya, S. Longhi, and L. Feng, Science **365**, 1163 (2019).